PAPER

Carbon supported Pd–Cu nanoalloys: support and valence band structure influence on reduction and oxidation reactions†

Marcus V. Castegnaro, [ID] [a] Andreia Gorgeski,[a] Maria C. M. Alves [ID] [b] and Jonder Morais [ID] *[a]

The present study has tracked the changes in the electronic and structural properties of Pd–Cu nanoalloys that were influenced by the composition and chosen support. Carbon supported Pd–Cu nanoalloys (Pd_xCu_{1-x}/C for x = 1, 0.7, 0.5, 0.3 and 0) were subjected to sequential thermal treatments (up to 450 °C) to induce reduction and oxidation reactions. Valence band photoemission data and *in situ* XAS results showed that stronger oxygen–metal bonds are formed in Cu-richer samples. A regeneration process assisted by the support was observed during the oxidation reaction, and its reduction efficiency was found to be dependent on the distribution of occupied electronic states near the Fermi level.

Introduction

The escalating research efforts to produce and characterize metal nanoalloys are due to their attractive size-induced properties, which are important for the development of new systems and applications. The possibility of tailoring their chemical and physical properties through the choice of the nanoalloy composition and atomic arrangement creates a quite exciting research field.[1–9] In this regard, compositional effects on the electronic and structural properties of Pd-based and Pt-based nanoalloys have been intensively studied.[5–10] In a recent study of carbon-supported Pd–Cu nanoparticles[9] we have demonstrated that alloying is able to prevent surface oxidation due to air exposure, while the higher the amount of Pd in the nanoalloy the less oxidized are both the Pd and the Cu atoms. Additionally, *in situ* XANES experiments demonstrated that the required temperature for the complete reduction of the nanoalloys depends on their composition.

This work presents new findings on the reactivity of Pd_x-Cu_{1-x}/C systems under both oxidizing and reducing atmospheres, contributing to deepen the understanding of the thermal stability of these nanoalloys and to provide tools to design future PdCu-based materials. Hence, three selected samples ($Pd_{0.7}Cu_{0.3}$/C, $Pd_{0.5}Cu_{0.5}$/C and Cu/C) were alternately exposed to CO and synthetic air flows under heating up to 450 °C.

The changes in the short-range order and in the chemical environment were investigated by *in situ* XAS measurements at the Cu K edge (8979 eV). Additionally, the gaseous products of the reactions were analyzed by *in situ* mass spectrometry. Briefly, the whole experiments were performed in three steps: (i) heating from room temperature (RT) to 450 °C under a CO flow, then cooling back to room temperature (RT) under a He flow; (ii) heating from RT to 450 °C under a synthetic air flow; and (iii) exposure to a CO flow at 450 °C, and then cooling to RT under a He flow. Time-resolved XANES spectra were collected during each step, and EXAFS spectra were acquired before and after each step. Valence band photoemission experiments shed some light on the correlation between the catalytic activities and density of occupied states near the Fermi edge.
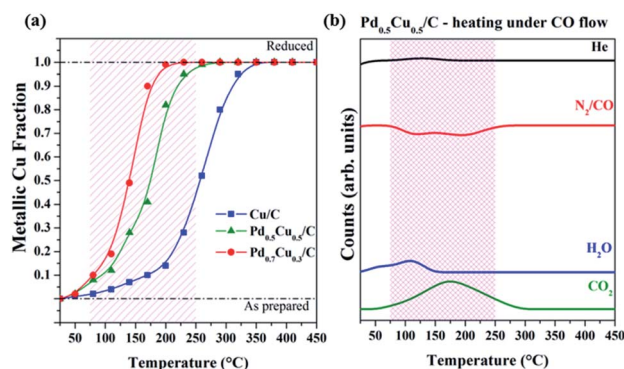

Fig. 1 (a) Temperature dependence of the metallic Cu fraction of Pd_xCu_{1-x}/C samples during heating under a CO flow. (b) Mass spectrometry results of major compounds formed during the heating of $Pd_{0.5}Cu_{0.5}$/C under a CO flow.

[a]*Instituto de Física-Laboratory on Electron Spectroscopy (LEe) – UFRGS, Porto Alegre 91501-970, RS, Brazil. E-mail: jonder@if.ufrgs.br*

[b]*Instituto de Química-UFRGS, Porto Alegre, 91501-970, RS, Brazil*

Results and discussion

During the first reaction step, the as-prepared samples were reduced by CO and the changes that occurred in the vicinities of the Cu atoms were observed *via* XANES data. The *in situ* XAS spectral evolutions of the Pd_xCu_{1-x}/C samples during the reaction with CO along with the XANES spectra of the selected references are available in the ESI.† The quantification of metallic Cu contribution in every spectrum was obtained *via* linear combinations of the initial and the final spectra of each sample.

The fraction of metallic Cu atoms for the nanoalloys exposed to CO evolved with temperature, as shown in Fig. 1(a). As previously verified for a wider range of compositions,[9] Pd-rich samples required lower temperatures to be completely reduced when compared to Cu-rich ones.

The mass spectrometry signals of the major compounds detected during this first step of the experiment (Fig. 1(b)) for the $Pd_{0.5}Cu_{0.5}/C$ sample indicated that the reduction reaction observed by XANES is tied to the CO_2 formation and concomitant CO decrease. This should be the expected behavior, since the oxygen atoms react with CO generating CO_2 *via* the CO + $O_{bond} \rightarrow CO_2$ reaction, where O_{bond} arrives from the oxidized metal sites. Considering that initially the supported nanoparticles are oxidized (M_xO_y/C) and the reaction with an excess of CO removes oxygen and generates CO_2, the simplified chemical reaction that took place during the first step of the experiment is as follows:

$$M_xO_y/C + CO \rightarrow xM/C + yCO_2 \ (M = Cu, Pd, PdCu) \quad (1)$$

Since the same reaction takes place for all samples, it is noteworthy that the reduction reaction depends on the alloy composition and the Pd amount influences the onset temperature. The sample with a higher Pd content requires a lower temperature to reduce the copper atoms. In a nutshell, weaker oxygen–metal bonds are present in Pd-richer carbon-supported nanoalloys while for Cu-richer carbon-supported nanoalloys stronger bonds are formed.

The Fourier transforms (FT) obtained from the Cu K edge EXAFS signals of the Pd_xCu_{1-x}/C samples are presented in Fig. 2. The FTs of some reference samples are available in the ESI.† The two upper signals of each graph in Fig. 2, which correspond to the as-prepared and the reduced samples, allow observation of the decrease of Cu–O bonds after CO reduction. Such changes are reflected in the structural parameters extracted from the EXAFS analyses (available in Tables SI1–3 in the ESI†) and corroborate the reduction process observed by XANES.

Once reduced, the samples were cooled down to RT. Then, the second step of the experiment was initiated, *i.e.*, the samples were exposed to the synthetic air flow while being heated up to 450 °C and, then, kept at that temperature for 40 mins, still under a synthetic air flow (Fig. 3(a)–(c) for samples Cu/C, $Pd_{0.5}Cu_{0.5}/C$ and $Pd_{0.7}Cu_{0.3}/C$, respectively). During this experiment step, the exposure of the reduced samples to synthetic air leads to the oxidation of the nanoparticles, as follows.

$$M/C + x/2O_2 \rightarrow MO_x/C \ (M = Cu, Pd, PdCu) \quad (2)$$
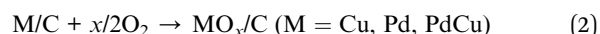
The XANES evolution (Fig. 3) shows that all samples were subjected to an oxidation process during the exposure to air, however with distinct behavior. This can be clearly observed in Fig. 4(a–c), which summarizes the linear combination results of all *in situ* XANES spectra collected during the second step of the experiment. The spectra used in each linear combination are highlighted and labelled in the respective graphs of Fig. 3, and more details on these analyses can be found in the Experimental section.

A remarkable difference is observed between the monometallic and bimetallic samples when heated under a synthetic air flow; the oxidation of Cu/C started at lower temperatures
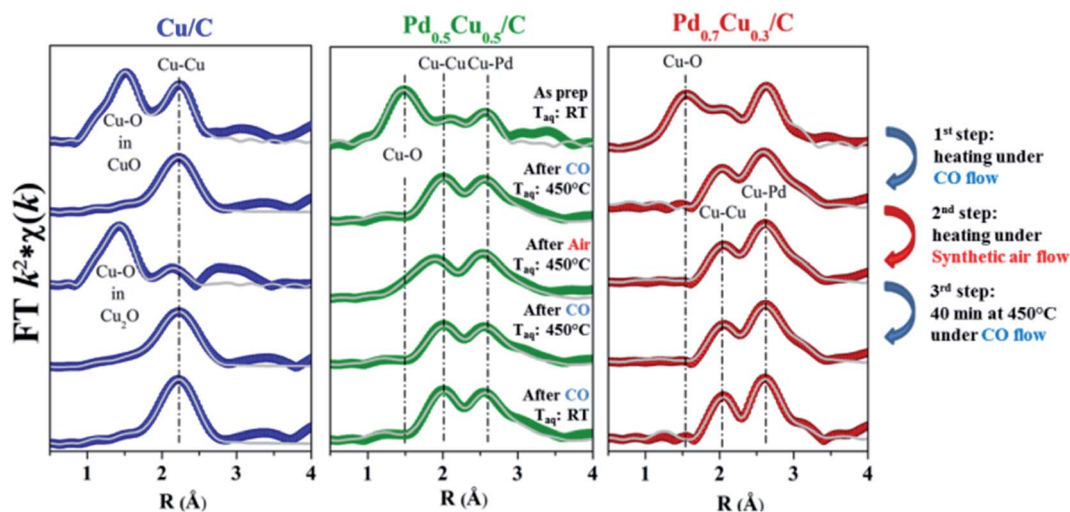

Fig. 2 Cu K edge EXAFS analyses: FT of k^2-weighted EXAFS signals collected after each step of reaction for all samples. The experiment steps and the acquisition temperatures are indicated in the spectra. The closed circles correspond to the experimental data and the grey continuous lines are the best obtained fits.

(Fig. 3(a–c) and4(a–c)) indicating an oxidation resistance promoted by alloying. Thereby, this complements previous X-ray photoelectron spectroscopy results[9] for as-prepared Pd–Cu nanoalloys that correlated the degree of oxidation at room temperature with the sample composition.

The oxidation reaction discussed above occurred during heating up to about 380 °C, but at higher temperatures all samples participate in a reduction process although with slightly different behavior. Fig. 3(c) and 4(c) demonstrate that this reduction process required a narrower range of temperatures to bring $Pd_{0.7}Cu_{0.3}/C$ back to its reduced initial state. Once the reduced state was reached, the sample presented no further changes during the next 40 minutes while kept at 450 °C under an air flow. The complete reduction is also corroborated by the EXAFS structural parameters obtained for this Pd-rich nanoalloy (Fig. 2 and Table SI3 in the ESI†).

In the case of $Pd_{0.5}Cu_{0.5}/C$ (Fig. 3(b) and 4(b)), the process required a wider temperature range although it did not lead to a completely reduced state. Even after 40 minutes at 450 °C, the sample maintained some degree of oxidation, as can be observed from the XANES linear combination and the EXAFS analysis. Further heating under a CO flow was able to quickly reduce the Cu atoms to the metallic state, as shown in Fig. SI5, in the ESI.†

It is remarkable that no significant structural changes were observed for both nanoalloy samples during the whole experiment. Despite the possibilities of phase segregation within the NPs driven by heat-treatments (e.g., formation of core–shell structures, segregated islands within the bimetallic NPs, or segregated monometallic NPs), the structural parameters extracted from the EXAFS data analysis evidenced that no clear atomic rearrangement took place during both the reduction and oxidation processes, as observed for other bimetallic systems.[13] This proves the thermal stability of the PdCu alloy structure presented in this work.

A closer examination of the monometallic sample oxidation kinetics brings out interesting results. Comparing some selected XANES spectra collected during its heating in air (for instance, those presented in Fig. SI4 in the ESI†) with some Cu-based references spectra (Fig. SI2 in ESI†), it is clear that the Cu atoms presented three distinct oxidation states at different stages of the reaction. The majority of the Cu atoms went from Cu^0 to Cu^{2+} while ramping up to about 350 °C. Then, a partial reduction took place and the final Cu^+ state was reached. The concordance between the XANES structures observed in the spectra collected at 350 °C and that of CuO, as well as between the XANES spectra of Cu_2O and those collected at the end of the reaction with air, corroborates the chemical state evolution described above. Accordingly, the reduction observed for the nanoalloys also takes place with Cu/C yet it was not able to completely reduce the sample due to the stronger oxygen bonds formed with pure copper.

To elucidate such an unusual reduction process occurring under an oxidizing atmosphere, mass spectrometry measurements were carried out while sample $Pd_{0.5}Cu_{0.5}/C$ was heated in air. These results are presented in Fig. 4(d) and can be
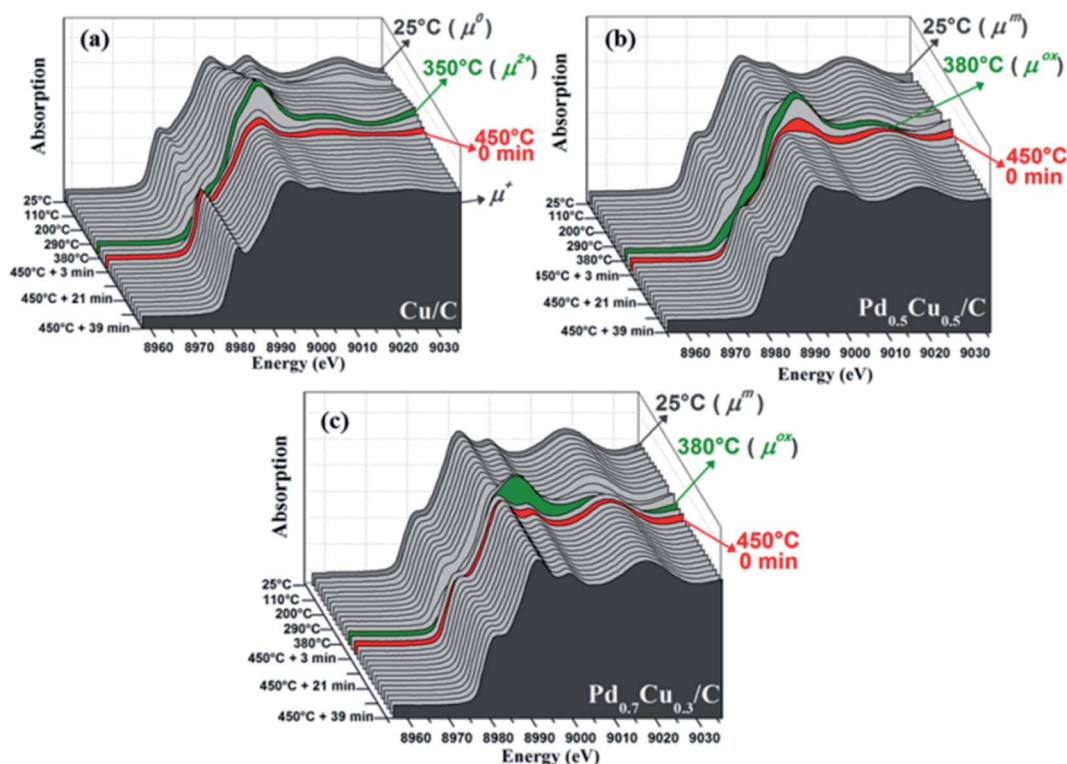

Fig. 3 Oxidation reaction with synthetic air: evolution of the Cu K edge XANES spectra of Cu/C (a), $Pd_{0.5}Cu_{0.5}/C$ (b) and $Pd_{0.7}Cu_{0.3}/C$ (c) presented as a function of temperature (during the heating up to 450 °C) and time (while the samples were kept at 450 °C).
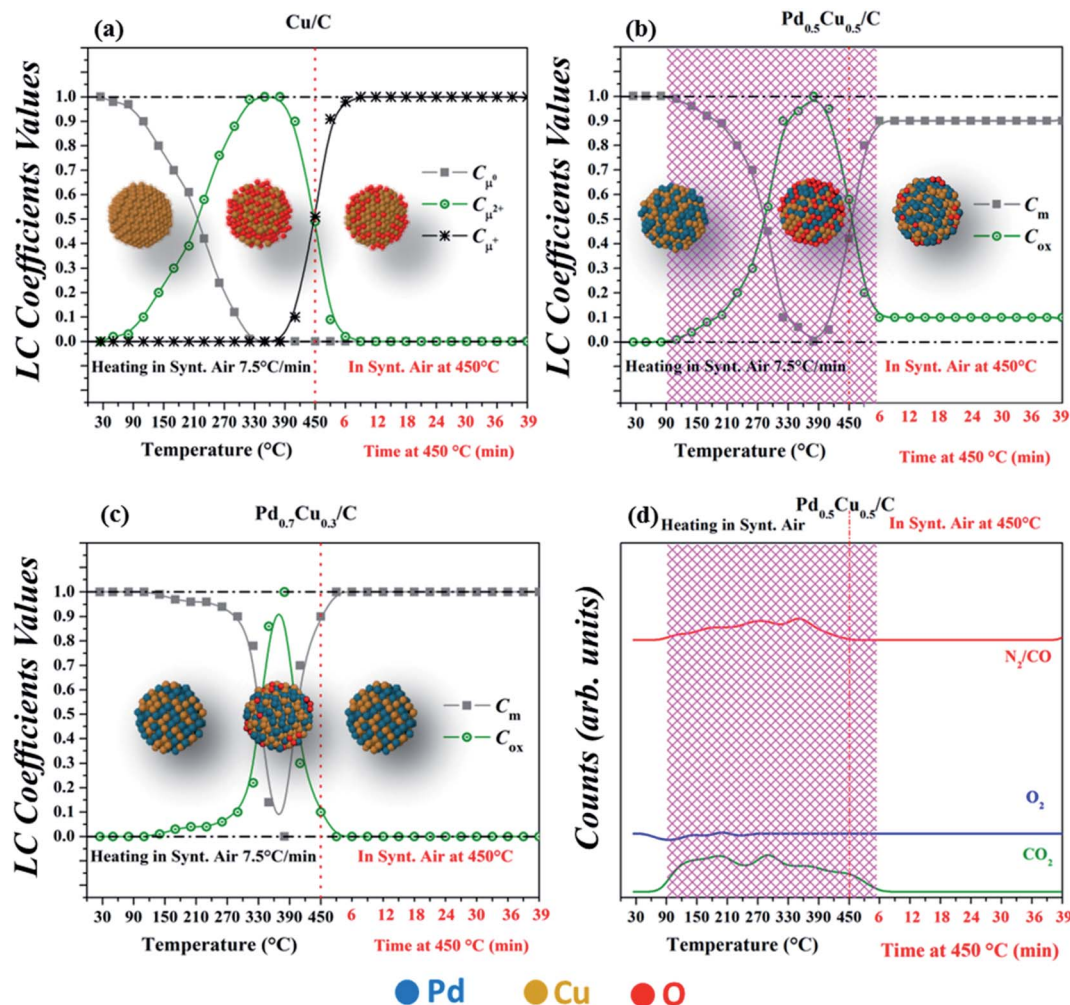
Fig. 4 Oxidation reaction with synthetic air: evolution of the coefficients employed for the linear combination of the XANES spectra of Cu/C (a), $Pd_{0.5}Cu_{0.5}$/C (b) and $Pd_{0.7}Cu_{0.3}$/C (c) presented as a function of the temperature (during the heating up to 450 °C) and of time (while the samples were kept at 450 °C), and (d) the mass spectrometry counts of major compounds observed during the heating under a synthetic air flow of $Pd_{0.5}Cu_{0.5}$/C.

compared to the results extracted from the XANES analysis (Fig. 4(b)) showing that simultaneously to the reduction onset, some CO_2 is detected in the exhaust gases. Since no CO, CO_2 or hydrocarbons were present in the reaction gas, the C atoms required to form the CO_2 originated from the support.

Thus, the reduction described here is similar to that observed during the partial self-regeneration of activated carbon-supported Pd[11], Pt[12] and PtPd[13] nanoparticles during NO direct decomposition, being related to the carbonaceous nature of the support. Similar behaviors have been described for several other metals as well.[14–16] In all situations, bonded oxygen atoms are assumed to take part in the CO_2 formation, resulting in the reduction of these metallic sites. The present results indicate that only bonded oxygen is available to form CO_2, since no significant CO_2 production was observed before and after the samples' reduction. Additionally, it was verified that the richer in Pd the sample is, the easier the O desorption is, resulting in a complete reduction of $Pd_{0.7}Cu_{0.3}$/C and in a partial reduction of $Pd_{0.5}Cu_{0.5}$/C. Such support-induced reduction also happens
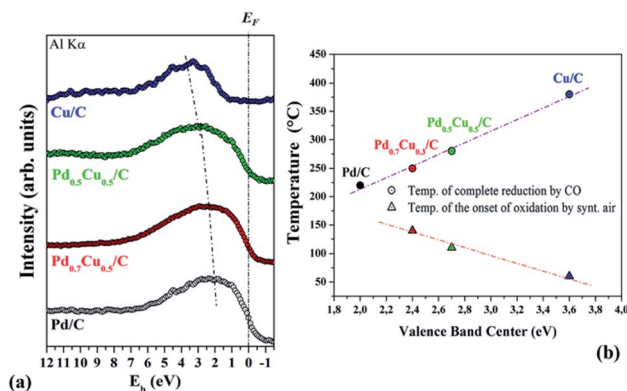

Fig. 5 (a) Valence band photoemission spectra for the as-prepared Cu/C, $Pd_{0.5}Cu_{0.5}$/C, $Pd_{0.7}Cu_{0.3}$/C and Pd/C. (b) Relationship between the binding energy of the valence band center of each sample, the temperature for their complete reduction by CO and the onset temperature during oxidation in synthetic air.

for the monometallic case but it was unable to bring the Cu atoms to a metallic state, as discussed. It is well-established that the reactivity of metallic surfaces is correlated with the metal valence band center, width and filling. Particularly, the more distant from the Fermi level a metal valence-band center is, the weaker its interaction with molecular oxygen and several types of adsorbates.[17–22] Nonetheless, the energy barrier for the elementary reactions in the process is another relevant factor to deal with surface reactivity.[18,21] For instance, metals with low O_2 dissociation barriers such as Co and Cu strongly bind to oxygen. In opposition, noble metals involve high energy barriers in the dissociative adsorption of O_2 and weak bonds are developed.[17,18,21] Thus, the compromise between the reaction barrier for the O_2 dissociation and the strength of the surface interaction with oxygen dictates whether oxygen interacts with a metal surface establishing weaker or stronger bonds during oxidation and reduction reactions. These properties are affected by the surface electronic structure;[17,22] therefore a simple correlation between the electronic structure and the reactivity of real catalysts may be difficult to state.

Our former investigations on Pd–Cu nanoalloys have demonstrated that the electronic structure of these systems is affected by the composition.[9] Additionally, the nanoalloys' valence band electronic configuration was proven to affect directly their reactivity towards the oxygen reduction reaction (ORR) in an alkaline medium.[10] For this reason it is important to compare the valence band photoelectron spectra of all the studied samples in order to ascertain modifications in the electronic properties due to alloying. The comparison between the valence band photoelectron spectra of $Pd_{0.5}Cu_{0.5}$/C and $Pd_{0.7}Cu_{0.3}$/C, and those of their monometallic counterparts (Cu/C and Pd/C) (Fig. 5(a)) clearly shows that the composition affects the valence band structure of the Pd_xCu_{1-x}/C samples. The samples with more Pd have valence band centers closer to the Fermi level.

To deepen the understanding of the behavior of the Pd_x-Cu_{1-x}/C system during the reduction and oxidation reactions investigated here, the temperature of the complete reduction by CO (extracted from Fig. 1(a)) and the onset temperature for the oxidation process under synthetic air (extracted from Fig. 4(a–c)) were plotted as functions of the binding energy of the valence band center. Assuming that the temperature required for the complete reduction is indicative of the energy involved in the reduction by CO, the data in Fig. 5(b) show that the lower the binding energy of the valence band center (*i.e.*, the higher the amount of Pd present in the sample) is, the higher the energy required to fully reduce the sample. Furthermore, taking the onset of the oxidation process as an indicator of the energy involved in the oxidation process due to synthetic air exposure, the comparison between the three samples points out that those containing more Cu (*i.e.*, with lower binding energy of the valence band center) are more easily oxidized by air.

Experimental

The Pd–Cu nanoalloys were prepared *via* wet chemical reduction of $PdCl_2$ and $CuCl_2$, employing trisodium citrate and ascorbic acid as stabilizing and reducing agents. The fresh colloids have been adsorbed on Vulcan XC-72R. Additional synthesis details can be found in ref. 9.

The *in situ* XAS experiments were performed at the XAFS1 beamline[23] of LNLS. The XAS spectra were collected in transmission mode at the Cu K edge (8979 eV) using a Si(220) channel-cut crystal, and standard Cu foil as an energy reference. Prior to the experiments, the samples were pressed into homogeneous pellets and placed in a tubular furnace where the reactions were carried out. The experiments were carried out in three steps:

(I) The samples were heated at a constant rate (7.5 °C min⁻¹) from room temperature to 450 °C under a CO flow (5% CO in He, 300 mL min⁻¹). Once the final temperature was reached, the samples were kept for 40 minutes. Then, the CO flow and the heating were turned off and the samples were cooled to RT under a He flow (300 mL min⁻¹).

(II) The samples were heated (7.5 °C min⁻¹) from RT to 450 °C under a synthetic air flow (300 mL min⁻¹). Once the final temperature was reached the samples were kept at 450 °C for 40 min under a synthetic air flow.

(III) The samples were exposed to a CO flow (5% CO in He, 300 mL min⁻¹) at 450 °C for 40 min and then cooled to RT under a He flow (300 mL min⁻¹).

Step I was also carried out under the same conditions for the Pd/C sample, and the corresponding XANES spectra were collected at the Pd K edge (24 350 eV) using the XDS beamline[24] of LNLS.

The detailed description of the XAS data acquisition and analysis procedures is available in the ESI.†

XPS measurements were carried out with Al Kα radiation (200 W, 14 kV, 15 mA). The valence band photoelectron spectra were acquired in a SPECS system equipped with a Phoibos 150 1D-DLD hemispherical electron analyser adjusted with a pass energy of 30 eV, an energy step size of 0.1 eV and an acquisition time of 0.5 s. The analyser's energy calibration was performed using the Au $4f_{7/2}$ peak (84 eV [25]), measured from clean Au foil.

Conclusions

This comprehensive study on the reactivity of carbon-supported Pd–Cu nanoalloys, combining *in situ* XAS and valence band photoemission results, states that oxygen atoms bond more easily and strongly to Cu-rich samples than to Pd-rich ones. Besides demonstrating the high thermal stability of the nanoalloys, we presented evidence that the samples under oxidation participate in a support-assisted regeneration process, which is based on the reduction of metal sites by carbon and results in the production of CO_2. This process revealed the contribution of the carbonaceous support to the sample behavior and a compositional-dependent reactivity and oxidation resistance. This could lead to applications in several fields thanks to their tunable oxidation resistance and to their electronic and structural properties, which are adjustable through the composition choice. Further studies will be conducted aiming at the elucidation of the support-assisted regeneration and its temperature dependence.

Author contributions

J. M. supervised the work. M. V. C. and A. G. carried out the experiments, collected and analysed the data. M. V. C, A. G., M. C. M. A. and J. M. discussed and interpreted the results and wrote the manuscript.

Conflicts of interest

There are no conflicts to declare.

Acknowledgements

References

1 R. Ferrando, J. Jellinek and R. L. Johnston, *Chem. Rev.*, 2008, **108**(3), 845–910.

2 S. Guo, S. Zhang and S. Sun, *Angew. Chem., Int. Ed.*, 2013, **52**(33), 8526–8544.

3 M. K. Debe, *Nature*, 2012, **486**(7401), 43–51.

4 Y. Wang, N. Zhao, B. Fang, H. Li, X. T. Bi and H. Wang, *Chem. Rev.*, 2015, **115**, 3343–3467.

5 K. D. Gilroy, A. Ruditskiy, H. Peng, D. Qin and Y. Xia, *Chem. Rev.*, 2016, **116**, 10414–10472.

6 T. Chen and V. O. Rodionov, *ACS Catal.*, 2013, **6**, 4025–4033.

7 L. Bu, S. Guo, X. Zhang, X. Shen, D. Su, G. Lu, X. Zhu, J. Yao, J. Guo and X. Huang, *Nat. Commun.*, 2016, **7**, 11850.

8 S. K. Sengar, B. R. Mehta and G. Gupta, *Appl. Phys. Lett.*, 2011, **98**(19), 193115.

9 M. V. Castegnaro, A. Gorgeski, B. Balke, M. C. M. Alves and J. Morais, *Nanoscale*, 2016, **8**(1), 641–647.

10 M. V. Castegnaro, W. J. Paschoalino, M. R. Fernandes, B. Balke, M. C. M. Alves, E. A. Ticianelli and J. Morais, *Langmuir*, 2017, **33**, 2734–2743.

11 M. V. Castegnaro, A. S. Kilian, I. M. Baibich, M. C. M. Alves and J. Morais, *Langmuir*, 2013, **29**(23), 7125–7133.

12 M. V. Castegnaro, J. Alexandre, I. M. Baibich, M. C. M. Alves and J. Morais, *Mater. Res. Express*, 2014, **1**, 044001.

13 D. Schafer, M. V. Castegnaro, A. Gorgeski, A. Rochet, V. Briois, M. C. M. Alves and J. Morais, *Phys. Chem. Chem. Phys.*, 2017, **19**, 9974–9982.

14 K. Almusaiteer, R. Krishnamurthy and S. S. C. Chuang, *Catal. Today*, 2000, **55**, 291–299.

15 M. J. Illan-Gomez, E. Raymundo-Pinero, A. Garcia-Garcia, A. Linares-Solano and C. S. M. de Lecea, *Appl. Catal., B*, 1999, **20**, 267–275.

16 M. J. Illan-Gomez, A. Linares-Solano, L. R. Radovic and C. S. M. de Lecea, *Energy Fuels*, 1996, **10**, 158–168.

17 W. J. Tang and G. Henkelman, *J. Chem. Phys.*, 2009, **130**(19), 194504.

18 B. Hammer and J. K. Norskov, *Surf. Science*, 1995, **343**, 211–220.

19 B. Hammer and J. K. Norskov, *Adv. Catal.*, 2000, **45**, 71–129.

20 J. Greeley, J. K. Nørskov and M. Mavrikakis, *Annu. Rev. Phys. Chem.*, 2002, **53**, 319–348.

21 Y. Xu, A. V. Ruban and M. Mavrikakis, *J. Am. Chem. Soc.*, 2004, **126**, 4717.

22 J. Greeley and M. Mavrikakis, *Nat. Mater.*, 2004, **3**, 810–815.

23 H. C. N. Tolentino, A. Y. Ramos, M. C. M. Alves, R. A. Barrea, E. Tamura, J. C. Cezar and N. Watanabe, *J. Synchrotron Radiat.*, 2001, **8**, 1040–1046.

24 F. A. Lima, M. E. Saleta, R. J. S. Pagliuca, M. A. Eleoterio, R. D. Reis, J. Fonseca Jr, B. Meyer, E. M. Bittar, N. M. Souza-Neto and E. Granado, *J. Synchrotron Radiat.*, 2016, **23**, 1538–1549.

25 J. F. Moulder, W. F. Stickle, P. E. Sobol and K. D. Bomben in, *Handbook of X-Ray Photoelectron Spectroscopy*, ed. J. Chastain, Perkin-Elmer Corporation, Eden Prairie, MN, 1992.